Efficient removal of nanoplastics from water using mesoporous metal organic frameworks

Daniel Pedrero[1], Carlos Edo[2], Francisca Fernández-Piñas[2,3], Roberto Rosal[1], Sonia Aguado[1,*]

[1]Department of Chemical Engineering, Universidad de Alcalá, E-28871 Alcalá de Henares, Madrid, Spain
[2]Department of Biology, Faculty of Science, Universidad Autónoma de Madrid, E-28049, Madrid, Spain
[3]Centro de Investigación en Biodiversidad y Cambio Global, Universidad Autónoma de Madrid. Darwin 2, 28049 Madrid, Spain

Abstract

Nanoplastics have garnered significant global attention as emerging environmental contaminants due to their susceptibility to be internalized by organisms, potentially leading to higher ecological and health risks compared to microplastics. Recently, adsorption has emerged as a promising strategy for nanoplastic removal, and new adsorbents have demonstrated impressive performance in this regard. In this study, we focused on the removal of polystyrene nanoplastics (NPs) from aqueous environments using a series of mesoporous Metal Organic Frameworks (MOFs). We synthesized mesoporous UiO-66 and its derivatives (–OH and $–NH_2$) through direct solvothermal synthesis in the presence of cetyltrimethylammonium bromide (CTAB) or Pluronic-type triblock copolymer (P123). The resulting materials had high crystallinity and displayed a hierarchical mesoporosity. Remarkably, we found that UiO-66-NH_2/P123 demonstrated exceptional efficiency in removing NPs, achieving up to 100 % removal efficiency at an initial concentration of 1 g L^{-1}. This indicates its potential as a highly effective adsorbent for nanoplastic removal from aqueous media.

1. Introduction

The use of plastics has transformed our society. Plastics are cheap, light materials, suitable to produce a wide variety of goods, and are less energy consuming than alternatives such as glass, metals or even paper. Consequently, the use of plastics has been rapidly increasing since the start of its industrial production in the 1950s. However, the increasing use of plastics is accompanied by a parallel increase in plastic waste [1]. Plastic particles are defined by their size, the main factor determining their environmental fate. Conventionally, plastic debris fragments are defined as microplastics (MPs) if their longest dimension is < 5 mm [2,3]. The lower limit of PMs is generally taken as 1 µm below which particles are considered nanoplastics (NPs) provided that they are produced from the degradation of larger particles and show colloidal behavior in aqueous matrices. The accumulation of plastic fragments (biodegradable or not) in the environment represents a great concern for the ecosystem and human health [4]. NPs can exhibit toxicity to a range of aquatic organisms by interfering basic biological processes such as feeding, reproduction, and growth. NPs are also suspect to impact human health upon internalization and accumulation in different tissues and organs, potentially leading to long-term health effects. Besides, as persistent pollutants, NPs can remain in environment for many years [3,5,6].

Due to their small size, the detection and removal of NPs from aqueous matrices pose significant challenges. To improve water quality, various techniques are employed. NPs can be effectively eliminated from water using various methods, including adsorption, coagulation/flocculation, flotation, filtration, magnetic separation, electrochemistry-based, advanced oxidation processes, photolysis, and photocatalysis. Although conventional methods like sedimentation, coagulation, and sand filtration are cost-effective, their limitations have spurred the development of novel approaches that are more effective in removing and monitoring these emerging contaminants [6-14]. Among these approaches, adsorption stands out due to its cost-effectiveness, wide applicability, and ease of implementation. Over the past years, diverse adsorbents such as biochar, protein sponges, and metal hydroxides have been developed specifically for the adsorption of NPs [15,16]. Sand filters integrated with activated carbon [17] and aluminosilicate filters [18] are a viable treatment technology to remove plastics, but in the micro size range. There are few studies that mention the removal of NPs [19-21].

The properties of the porous materials, such as pore size, surface chemistry, and surface area, affect their adsorption capacity for NPs. The surface properties of the porous material, including its charge and functional groups, can also impact the adsorption

* Corresponding author: sonia.aguado@uah.es
Available online: November 29, 2023

process. If the NP particles are negatively charged, a positively charged porous material can enhance adsorption through electrostatic attraction. Also, the size and distribution of the pores in the porous material play a crucial role in determining the adsorption efficiency for NPs. Therefore, selecting porous materials with appropriate pore sizes and distributions can optimize their adsorption capacity for NPs. It is worth noting that the field of NPs adsorption with porous materials is still relatively new, and ongoing research aims to further explore the mechanisms and optimize the adsorption process. [22,23].

Conventional porous materials show microchannels or pores that are smaller than NPs and therefore might not be ideal adsorbents for NPs. Porous crystalline materials known as Metal Organic Frameworks (MOFs) have garnered significant attention in diverse fields such as gas storage, separation, catalysis, sensors, and contaminant removal [24-30]. These porous materials are formed by assembling metal ions and organic ligands. MOFs offer high porosity, tunable structures, and a wide range of functionalities. They possess the capacity to incorporate different metal centers, adjustable functional groups, and charge characteristics. The ability to tailor the structure of MOFs allows for the precise placement of functional groups in their structure. As a result, custom porous environments can be achieved at the molecular level through the proper choice of building blocks.

The development of MOFs to absorb NPs, is highly demanded, however, there are only a few reported studies on that topic. ZIF-67 demonstrates effective adsorption and removal of polystyrene (PS) from water [31]. The application of ZIF-8-based wood aerogel is effective in the removal of poly(1,1-difluoroethylene) and PS, exhibiting a notable efficiency in plastic removal [32]. In terms of composite materials, a proposed method involving nanopillared structures composed of 2D MOF intercalating carbon encapsulating FeO nanoparticles (C@FeO), enables removal of MPs [33]. Another example is zirconium MOF-based foam that achieves a removal rate of 95 % and demonstrates improved recyclable efficiency [34].

UiO-66 is a type of MOF material composed of inorganic metal nodes, typically zirconium (Zr), connected by organic linkers terephthalates [35]. The resulting three-dimensional structure forms a porous framework with a large surface area and a high degree of porosity. UiO-66 has gained significant attention in the field of materials science and chemistry due to its exceptional stability, high surface area, and tunable properties. UiO-66 can be modified by incorporating different chemical functions in the organic linker, leading to the creation of various derivatives with tailored properties.

Wang et al demonstrated that an enlarged mesoporous surface areas provide sufficient active sites for MPs adsorption [36]. Most MOFs are categorized as microporous, which implies pore dimensions typically around 2 nm. This intrinsic microporosity imposes limitations on some applications of MOFs. However, expanding the porosity of MOFs to the mesoporous range, where pore sizes cover from 2 nm to 50 nm, offers significant advantages. Such an extension enables MOFs to better meet the increasing demands in applications, particularly when it comes to the adsorption of NPs.

In this study, we present a novel method for synthesizing mesoporous UiO-66, which includes the introduction of a surfactant such as cetyl trimethyl ammonium bromide (CTAB) or P123. This synthetic strategy allows us to obtain mesoporous UiO-66 materials, along with their -OH and -NH_2 derivatives. Furthermore, we conducted a series of adsorption experiments for removal of PS NPs with a diameter of 26 nm.

2. Materials and methods

2.1 Synthesis

The synthesis reactions were performed using solvents as received. All remaining reagents, which were commercially accessible, were used without any additional purification. ZrCl4 (Merck), terephthalic acid (BDC, Aldrich), dihydroxyterephthalic acid (BDC-OH, Biosynth), 2-aminoterephthalic acid (BDC-NH_2, Aldrich), cetyl trimethyl ammonium bromide (CTAB, Aldrich), poly(ethylene oxide)-poly(propylene oxide)-poly(ethylene oxide) triblock copolymer template (Pluronic P123, Aldrich), 1,3,5-trimethylbenzene (TMB, Thermo Scientific), acetone, ethanol (EtOH) and N, Ndimethylformamide (DMF).

Mesoporous UiOs-66 specimens were prepared through a solvothermal approach, by adopting and modifying two previously reported methods utilized to induce mesoporosity in the structure of a different MOF. These methods involved the use of cetyl trimethyl ammonium bromide (CTAB) as a surfactant [37] and Pluronic P123 [38].

In the first synthesis, a mixture of $ZrCl_4$ (4.5 mmol) and BDC (4.5 mmol) or BDC-NH_2 (4.5 mmol) was added into 30 mL dimethylformamide (DMF). Then, CTAB (1.35 mmol) and TMB (0.675 mmol) were added while stirring. This mixture was then transferred into a Teflon-lined autoclave and heated in the oven at 120 °C for 48 h. In the case of UiO-66-OH, a mixture of $ZrCl_4$ (4.5 mmol) and BDC-OH (4.5 mmol) was added to 30 mL acetone. Then, CTAB (1.35

mmol) and TMB (0.675 mmol) were added while stirring. This mixture was then transferred into a Teflon-lined autoclave and heated in an oven at 100 °C for 24 h.

In the second synthesis, a mixture of $ZrCl_4$ (6 mmol), BDC (6 mmol) or BDC-NH_2 (6 mmol) and P123 (0.05 mmol) was added into 40 mL dimethylformamide (DMF) under stirring. This mixture was then transferred into a Teflon-lined autoclave and heated in the oven at 120 °C for 48 h. In the case of UiO-66-OH, a mixture of $ZrCl_4$ (6 mmol), BDC-OH (6 mmol) and P123 (0.05 mmol) was added into 40 mL acetone under stirring. This mixture was then transferred to a Teflon-lined autoclave and heated in an oven at 100 °C for 24 h.

For the sake of clarity and henceforth, the samples are designated as UiO-66-X/CTAB and UiO-66-X/P123, in accordance with synthesis involving CTAB and P123 respectively, where X represents either OH or NH_2. For comparison, microporous UiOs-66 were synthesized in the absence of surfactant.

Following each synthesis, the obtained solid was subject to a triple washing process using EtOH and subsequently dried in an oven at 100 °C. To eliminate surfactant, two methods were used: either the samples were extracted with EtOH in a Soxhlet apparatus at 80 °C for 12 h, or subject to vacuum outgassing at 200 °C for 12 h.

2.2 Characterization

XRD measurements were recorded in the 10-50° 2θ range (scan speed = 20 s, step = 0.04°) by powder X-Ray diffraction (PXRD) using a Shimadzu 600 Series Diffractometer employing CuKα radiation (λ = 1.5418 Å). XRD measurements were recorded before surfactant removal.

FTIR spectra were obtained in a Thermo-Scientific Nicolet iS10 with a Smart iTR-Diamond ATR module. Spectra were taken in the 4000–800 cm^{-1} range with a resolution of 4 cm^{-1} (data spacing of 0.483 cm^{-1}) using 32 scans.

Transmission electron microscopy (TEM) studies were carried out on a JEOL JEM 2100 electron microscope operating at 200 kV. The samples for TEM were mounted on a microgrid carbon polymer supported on a copper grid by placing a few droplets of a suspension of sample in isopropanol on the grid, followed by drying at ambient conditions. Fluorescent pictures were captured in a LEICA TCS-SP5 confocal microscope. Scanning electron microscopy (SEM) studies were carried out on a JEOL JSM 7600F.

The N_2 adsorption/desorption isotherms at 77 K were measured on a Beckman Coulter SA 3100. The samples are outgassed under vacuum before start of the measurements. The specific surface is determined by BET method (Brunauer-Emmett-Teller), the micropore volume by t-plot analysis, and the mesopore volume by BJH.

Surface Zeta potential measurements were performed using dynamic light scattering in a Zeta-Sizer Nano Series (Malvern Instruments Ltd.). Measurements are performed at 25 °C using comparable amounts of MOF in ultrapure water. The pH of the MOF suspension was recorded using a Crison 25 + pH-meter.

2.3 Adsorption process

The NPs used in this work were Fluoro-MaxTM PS NPs (Thermo Scientific). These particles have a nominal diameter of 26 nm (confirmed by DLS analysis, Figure S1, Supplemantaty Materials, SM) and incorporate a non-leaching green, fluorescent dye. The fluorochrome has an excitation maximum of 468 nm and emitted at 580 nm. The fluorescence was quantified using a Fluoroskan Ascent FL fluorimeter (Thermo Scientific) equipped with Ascent Software.

In order to evaluate the MOFs retention capacity, a series of experiments were conducted by exposing the MOF materials to NPs dispersed in ultrapure water. A concentration of 2.5 g L^{-1} was chosen for the MOF, while the NPs were tested at concentrations of 0.02 g L^{-1} and 1 g L^{-1}. In addition to the samples, negative controls for all materials and NPs samples were assessed following identical protocols.

The adsorption procedure was performed in glass vials at room temperature, employing a GFL 3005 shaker operating at 250–300 rpm. The contact between MOFs and NPs extended from 1 h to 168 h. After the contact period, the samples were extracted and filtered using 1 µm syringe filters (Whatman Puradisc 25 PTFE filters) to separate the MOF materials. The filtered solution was transferred to 96-well plates for fluorescence analysis. The concentration of NPs in the filtered solution was calculated from a calibration curve. We conducted leaching experiments to prove that the fluorescent compound of the nanospheres does not leach out from the plastic (Figures S2-S4, SM).

3. Results and discussion

3.1. Mesoporous UiOs-66

The preparation of mesoporous MOFs through direct combination of metal ions and ligands by standard solvothermal synthesis methods is challenging. Currently, only a limited number of examples exist where genuinely mesoporous MOFs exhibit well-defined and ordered pores throughout their extended

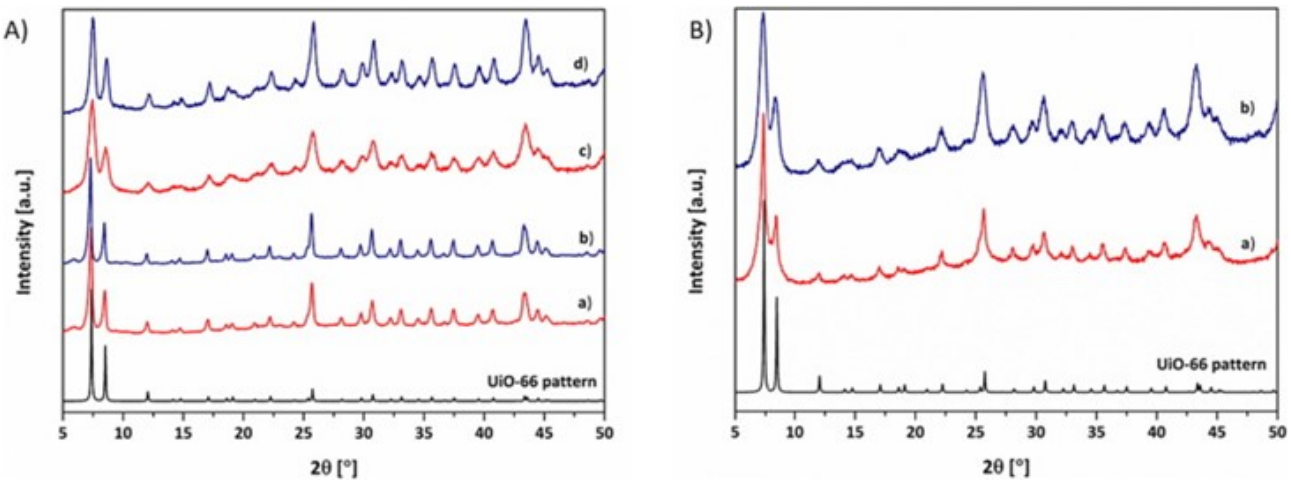

Figure 1: *A. PXRD patterns of (a) UiO-66/CTAB, (b) UiO-66/P123, (c) UiO-66-NH_2/CTAB, (b) UiO-66-NH_2/P123. B. PXRD patterns of (a) UiO-66-OH/CTAB, (b) UiO-66-OH/P123.*

structures. Synthetic strategies often rely on incorporating extended linkers and metal clusters. Nevertheless, the synthesis of elongated ligands typically involves multiple steps, adding complexity to the process. Unfortunately, open MOFs constructed using this method often find their pores occupied by guest molecules. Consequently, these guest molecules must be removed to establish a permanent porosity, a step that can potentially lead to structural collapses or instabilities within the MOF framework. An alternative approach involves applying a templating strategy to create mesopores within the existing microporous MOF. This strategy holds significant appeal as it results in materials with a hierarchical mesoporosity, offering additional structural complexity and enhanced functionality [39-41].

We modified the synthesis method for mesoporous UiOs-66 based on the approach used for mesoporous HKUST-1, which involved the use of CTAB [37] and P123 [38]. The changes include adjustments in the molar ratio of metal-ligand, as well as changes in synthesis temperature and time [35]. It is worth noting that attempts to prepare the material using alternative synthesis methods, such as those involving citric acid, tetramethylammonium hydroxide (TMAOH), or different metal–organic coordination assemblies, resulted in the formation of amorphous or poorly crystalline materials [42-44]. The X-ray diffraction (XRD) patterns of the synthesized materials (based on UiO-66 and UiO-66-NH_2) agreed with the simulated pattern of UiO-66 (Fig. 1A). Attempts to synthesize UiO-66-OH/CTAB and UiO-66-OH/P123 in DMF were unsuccessful, resulting in an amorphous powder. However, it is possible to prepare UiO-66 materials using various solvents. Consequently, we conducted the synthesis in acetone [34], resulting in the formation of crystalline materials that exhibited a PXRD consistent with UiO-66. (Fig. 1B).

From the Fourier Transform Infrared (FTIR) analysis (Figures S5-S7, SM), peaks at 3255 cm^{-1} and 3343 cm^{-1} highlight the likely presence of hydroxyl and amino groups in the UiO-66-OH and UiO-66-NH_2 samples. Peaks in 2950-2987 cm^{-1} region further suggest methylene or methyl group inclusions. The UiO-66 sample exhibits peaks at 1395 cm^{-1}, 1157 cm^{-1}, and 883 cm^{-1}, which align with methyl groups, potential ethers or esters, and aromatic structures. These spectral attributes are also apparent in UiO-66-OH and UiO-66-NH_2, suggesting a shared structural basis with the UiO-66 sample. However, minor differences are observable. A peak at 1120 cm^{-1} in the UiO-66-OH sample, deviating from conventional C-O stretch regions, might denote a modified hydroxyl group or a distinct molecular setting. Conversely, UiO-66-NH_2 demonstrates peaks that align with amines at 1158 cm^{-1} and 1100 cm^{-1}, with additional bands at 1337 cm^{-1} and 1258 cm^{-1} corresponding to C-N modes, hinting at amino group incorporation. In essence, despite a shared structural foundation across the samples, spectral deviations in UiO-66-OH and UiO-66-NH_2 reveal distinct chemical alterations, underscoring the introduction or adaptation of certain functional groups.

N_2 adsorption–desorption measurements at 77 K were conducted to investigate their textural parameters as summarized in Table 1. The corresponding isotherms are shown in Fig. 2. The data revealed that UiO-66-OH/P123, UiO-66-NH_2/CTAB, and UiO-66-NH_2/P123 (s and v) displayed the highest mesoporous volume. Mesoporous UiO-66 samples showed higher surface area compared to –OH and –NH_2 derivatives but lower mesoporous volume. The introduction of mesoporosity through CTAB or P123 did not significantly impact textural properties. Specifi-

Table 1. *Surface areas and pore volumes of mesoporous UiOs-66.*

Sample	Treatment[a]	S_BET [m^2 g^{-1}][b]	V_t [$cm^3 \cdot g^{-1}$][c]	V_{meso} [$cm^3 \cdot g^{-1}$]	V_{micro} [$cm^3 \cdot g^{-1}$][d]
UiO-66/CTAB	s	946	483	287	196
UiO-66/CTAB	v	977	492	272	220
UiO-66/P123	s	1015	432	207	325
UiO-66-OH/CTAB	s	433	213	134	78
UiO-66-OH/P123	s	634	766	683	83
UiO-66-NH_2/CTAB	s	583	623	541	82
UiO-66-NH_2/P123	s	714	528	378	150
UiO-66-NH_2/P123	v	506	340	260	80

(a) post-synthesis treatment: s = Soxhlet, v = vacuum outgassing; (b) BET specific surface area; (c) single point adsorption total pore volume at P/P_o = 0.99; (d) t-Plot micropore volume (V_{meso} is calculated by subtracting V_{micro} from V_t).

cally, for UiO-66-OH materials, samples synthesized with P123 exhibited higher mesoporous volume than those prepared with CTAB. Conversely, for UiO-66-NH_2 materials, the samples synthesized with CTAB had higher mesoporous volume than those synthesized with P123.

Pore evacuation method did not influence the results significantly as shown comparing sample UiO-66/CTAB with surface area 949 m^2 g−1 and 977 m^2 g−1 for Soxhlet extraction and vacuum outgassing, respectively. However, the sample UiO-66-NH_2/CTAB shows a larger mesoporous volume, indicating that its synthesis creates more mesoporosity compared to synthesis with P123. Additionally, in the case of materials with occluded P123, a more severe treatment might be necessary to remove all the trapped compounds. The better performance of neutral surfactants for the synthesis of materials with hierarchical porosity has been stated elsewhere [39].

Commonly used plastic materials like PS, polyethylene (PE), and polypropylene (PP) exhibit significant hydrophobic properties, what provides them an apparent negative charge. Zeta potential measures the effective electric charge on the surface of NPs. Consequently, the charge interactions between NP particles and adsorbents emerge as a crucial aspect of the adsorption process. A higher positive zeta potential proves to be more advantageous in the adsorption of negatively charged particles [45]. Only a few research studies have been conducted to explore the zeta potential of MOFs, revealing intriguing findings regarding the electrical charge exhibited by specific MOFs. From the representative MOFs, ZIF-8, MIL-101, UiO-66 and MIL-53 show a positively charged zeta potential, while HKUST-1 exhibits a negatively charged zeta potential [34, 46-49].

In order to assess the potential interaction between the synthesized MOF materials and NPs, we measured the zeta potentials of both MOF samples and PS NPs. As indicated in Table 2, all the synthesized mesoporous MOF samples exhibited a positive zeta potential (at slightly acid pH). Since the NPs possessed a negative zeta potential of -30 mV, the materials with higher electrostatic interaction with the NPs would be those with high positive charge. Among them, UiO-66-OH/CTAB and UiO-66-NH2/P123 displayed zeta potential values of + 32.6 mV and + 32.9 mV. The method of surfactant removal was shown to influence the obtained zeta potential, which was considerably higher in the samples that underwent vacuum outgassing.

Table 2. *Zeta potential of mesoporous UiOs-66.*

Sample	Treatment	Zeta potential [mV]
UiO-66/CTAB	s	+20.1 ± 1.2
UiO-66/CTAB	v	+29.3 ± 1.3
UiO-66/P123	s	+10.2 ± 0.9
UiO-66-OH/CTAB	s	+32.6 ± 1.7
UiO-66-OH/P123	s	+10.5 ± 2.2
UiO-66-NH_2/CTAB	s	+22.8 ± 1.7
UiO-66-NH_2/CTAB	v	+25.3 ± 1.7
UiO-66-NH_2/P123	s	+27.7 ± 0.8
UiO-66-NH_2/P123	v	+32.9 ± 2.6
Fluoro-MaxTM NPs	-	-30.0 ± 0.4

3.2. Adsorption removal of NPs

To assess the efficacy of retaining NPs in aqueous media, the samples were exposed to known concentrations of NPs. The experiments were conducted using NPs concentrations in the 20 mg L^{-1} g L^{-1} range. The higher NPs concentrations were used to provide accurate removal rates from fluorescence measurements and were necessary in view of the high adsorption capacity of the MOFs tested. Exposure times extended up to 1 week to ensure equilibrium.

Among the samples, those based on UiO-66-NH_2 exhibited a higher percentage of NPs capture com-

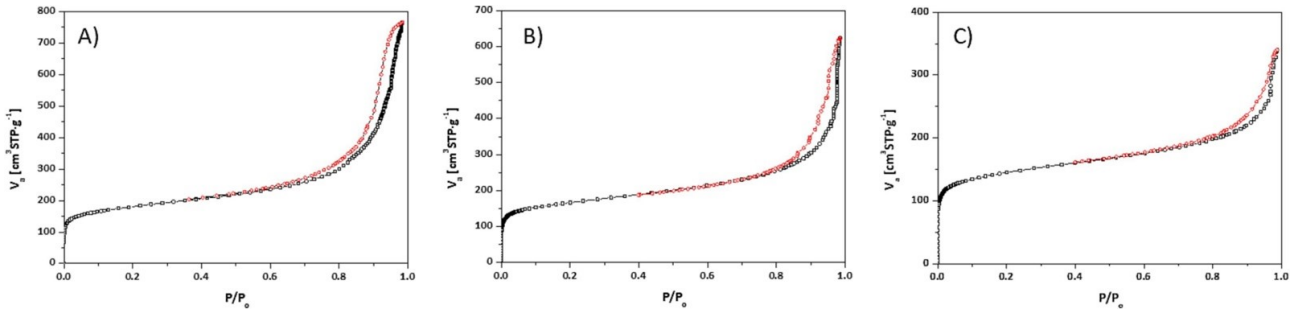

Figure 2: *Nitrogen isotherms at 77 K, (A) UiO-66-OH/P123; (B) UiO-66-NH_2/CTAB (s); and (C) UiO-66-NH_2/P123 (v).*

pared to those based on UiO-66-OH. In particular, sample UiO-66-NH_2/P123 (v) achieved 100 % retention after one week for an initial concentration of 1 g L^{-1}. These results agree with the assumption that the interaction between the positively charged MOFs and negatively charged NPs were mainly electrostatic, which might be the primary adsorption mechanism. The efficacy of NPs removal is influenced by factors such as zeta potential, mesoporosity, and BET surface area. However, obtaining a direct and straightforward deduction from these factors may pose a challenge.

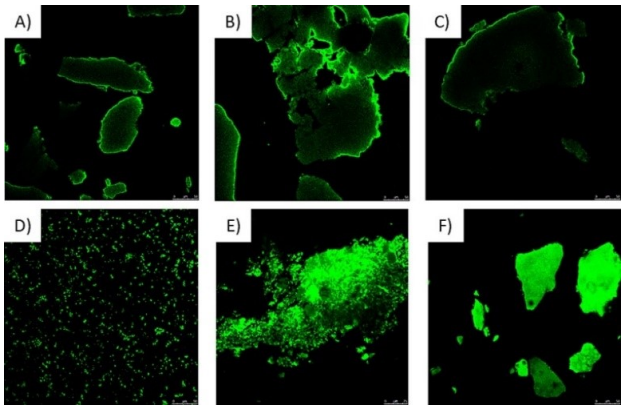

Figure 3: *Confocal fluorescence microscopy images of (A) UiO-66/CTAB (s), 3 h; (B) UiO-66/CTAB (v), 3 h; (C) UiO-66/P123 (s), 3 h; (D) UiO-66-OH/CTAB (s), 3 h; (E) UiO-66-OH/P123 (s), 1 week and (F) UiO-66-NH_2/P123 (v), 1 week.*

The results showed that the extent of NPs capture could be explained by the combined effect of the electrostatic interaction favoured by the positive surface charge of MOFs and the higher mesoporosity that provided adsorption sites with capacity to accommodate NPs in the tens of nm size range. For instance, UiO-66-OH/P123, with a zeta potential of + 10.5 mV and a mesoporosity of approximately 90 %, achieved a 39.9 % NPs removal, whereas UiO-66-OH/CTAB, with a higher zeta potential of + 32.6 mV but lower mesoporosity of 63 %, reached a similar removal rate of 40.5 %. For UiO-66-NH_2, there was a clear direct relationship between the zeta potential values and the capture percentage of NPs. The samples exhibit

Table 3. *Removal performance of mesoporous UiOs-66 (1 g L^{-1} NPs concentration, 1 week).*

Sample	Treatment	Removal (%)
UiO-66/CTAB	s	29.2
UiO-66/CTAB	v	6.9
UiO-66/P123	s	41.4
UiO-66-OH/CTAB	s	40.5
UiO-66-OH/P123	s	39.9
UiO-66-NH_2/CTAB	s	65.0
UiO-66-NH_2/CTAB	v	69.5
UiO-66-NH_2/P123	s	77.7
UiO-66-NH_2/P123	v	100

capture percentages of 65.0 %, 69.5 %, 77.7 %, and 100 % for zeta potential values of + 22.8 mV, +25.3 mV, +27.7 mV, and + 32.9 mV, respectively. Interestingly, UiO-66-NH_2/P123 (v) achieved the same capture rate of 100 %, even though it has a lower zeta potential compared to the original UiO-66-NH_2. This fact suggests that its high mesoporosity of 76 % compensated for the slightly lower zeta potential, resulting in equally efficient NP capture capacity compared to non-mesoporous UiO-66-NH_2 specimens.

In our study, we conducted a thorough comparison by evaluating the capture efficiency of MOFs at an initial concentration of 1 g L^{-1}, analyzing the material performance with a NP-to-MOF ratio of 1 gNPs $gMOF^{-1}$. The utilization of lower NP concentrations in earlier studies necessitated shorter contact times, typically between 12 and 24 h (Table 4). This was in accordance with the lower NP concentrations used, as the higher initial concentration of NPs employed in our work needs for a more prolonged interaction time between the MOFs and NPs. By employing a higher initial NP concentration, we sought to thoroughly investigate the removal capabilities of the mesoporous MOFs and explore their efficiency in capturing NPs under more challenging conditions. This approach provides valuable insights into the potential application of these MOFs as effective adsorbents for nanoparticle removal, particularly at

Table 4. *Comparison of plastic removal with solid porous adsorbents.*

Adsorbent	Plastic particles	Initial gNPs $gMOF^{-1}$	Contact time	Removal mgNPs $gMOF^{-1}$	Reference
Activated carbon	PS (90 nm)	0.008	4 h	2.2	[50]
MIL-101 (Cr)	PS (50–70 nm)	0.7	35 h 665	[51]	
Minerals PS	(50 nm)	0.01	5 h	7.5	[21]
Coffee grounds	PS (100 nm)	0.008	2 h	6	[20]
Biochar	PS (300 nm)	0.007	30 min	1.4	[19]
Mesoporous UiO-66 s*	PS (30 nm)	1	3 h, 1 week	33-524	This work

* UiO-66-NH_2/P123 (v).

higher NP concentrations encountered in real-world scenarios.

Confocal fluorescence microscopy allowed obtaining images of the fluorescent PS NPs attached onto MOFs. Fig. 3 displays the images of several MOF samples, exposed to PS NPs. The intensity of green fluorescence revealed the intensity of PS adsorption and surface coverage, which was clearly higher in sample UiO-66-NH_2/P123 (v), compared to UiO-66-OH/P123 (s), UiO-66/CTAB and UiO-66/P123 in agreement with the results of NPs adsorption shown in Table 3. The efficiency of the regeneration process for MOF samples is investigated through cycles of 30-minute contact with solvents, including EtOH, MeOH, and a 0.005 M NaOH solution. Examination of confocal fluorescence microscopy images taken before and after the regeneration process indicates its effectiveness (Figure S7, SM).

In order to assess how the inclusion of surfactant affects the final morphology and structure of the mesostructured samples obtained, we performed SEM and TEM analyses (Fig. 4). It is important to note that SEM produces surface images of the crystals, while TEM generates images of the internal structure. Despite this distinction, there are not significant differences in the crystal geometry of UiO-66-NH_2 before or after introducing mesoporosity. Additionally, it is essential to emphasize that the absence of perfect geometric faces in the crystals did not imply that the material lacks crystallinity. Through standard macroscopic techniques like X-Ray diffraction, we confirmed that the materials are indeed crystalline. TEM images reveal that NPs are not enter the mesopores of the material. Instead, it is probable that the NPs predominantly adhere to the external surface of the MOF. Despite this, the mesoporosity of the MOF plays a crucial role in augmenting the active surface area, thereby positively influencing the adsorption process. This phenomenon underscores the importance of mesoporosity in enhancing the overall adsorptive capacity of the MOF, even if NPs primarily interact with the external surface rather than entering the mesopores.

4. Conclusions

In this groundbreaking study, we thoroughly investigated the effectiveness of mesoporous UiO-66 for removing PS NPs from aqueous environments. For the first time, we successfully prepared mesoporous UiO-66 by incorporating either CTAB or P123 during the solvothermal synthesis process. The resulting samples exhibited a remarkable degree of crystallinity, preserving the original MOF structure. Furthermore, these synthesized materials demonstrated a mesoporous volume ranging from 50 to 90 % of the total pore volume. The as-synthesized mesoporous MOFs displayed a positive surface charge (zeta potential as high as +32.9 mV), which allowed electrostatic interaction with the negatively charged PS NPs (zeta potential -30.0 mV). In this work we obtained an exceptional removal efficiency that reached 100 % in the case of UiO-66-NH_2/P123 for a concentration ratio as high as 1:1 (mass concentration of PS NPs versus mass concentration of MOF). This result highlights the potential of UiO-66-NH_2/P123 as high-capacity adsorbent for the removal of NPs from aqueous matrices.

Acknowledgements

We gratefully acknowledge the financial support of the Spanish Ministry of Science and Innovation (MICINN), research projects PID2020-113769RB-C21/22, PLEC2021-007693 and TED2021-131609B-C32. We also thank ICTS-CNME (National Center for Electronic Microscopy of Spain) for technical assistance in SEM and TEM images.

References

[1] Plastics Europe, 2023. Plastics - the Fast Facts 2023. Plastics Europe, Brussels

[2] J. Gigault, A. Halle, M. Baudrimont, P. Pascal, F. Gauffre, T. Phi, H. El Hadri, B. Grassl, S. Reynaud, Current opinion: What is a nanoplastic? Environ. Pollut. 235 (2018) 1030-1034.

[3] D.M. Mitrano, P. Wick, B. Nowack, Placing nanoplastics in the context of global plastic pollution. Nat. Nanotechnol. 16 (2021) 491-500.

[4] R. Lehner, C. Weder, A. Petri-Fink, B. Rothen-Rutishauser, Emergence of nanoplastic in the environment and possible impact on human health. Environ. Sci. Technol. 53 (2019) 1748-1765.

[5] Y. Ju-Nam, J.R. Lead, Manufactured nanoparticles: An overview of their chemistry, interactions and potential environmental implications. Sci. Total Environ. 400 (2008) 396-414.

[6] V. Kumar, E. Singh, S. Singh, A. Pandey, P.C. Bhargava, Micro- and nano-plastics (MNPs) as emerging pollutant in ground water: Environmental impact, potential risks, limitations and way forward towards sustainable management, Chem. Eng. J. 459 (2023) 141568.

[7] Z. Chen, W. Wei, X. Liu, B.-J. Ni, Emerging electrochemical techniques for identifying and removing micro/nanoplastics in urban waters, Water Res. 221 (2022) 118846.

[8] S. Hamzah, L. Ying, A. Azmi, N. Razali, N. Hairom, N. Mohamad, M. Harun, Synthesis, characterisation and evaluation on the performance of ferrofluid for microplastic removal from synthetic and actual wastewater, J. Environ. Chem. Eng. 9 (2021) 105894.

[9] Q. Hou, M. Zhen, H. Qian, Y. Nie, X. Bai, T. Xia, M. Laiq Ur Rehman, Q. Li, M. Ju, Upcycling and catalytic degradation of plastic wastes, Cell Rep. 2 (2021) 100514.

[10] H. Luo, Y. Zeng, Y. Zhao, Y. Xiang, Y. Li, X. Pan, Effects of advanced oxidation processes on leachates and properties of microplastics, J. Hazard. Mater. 413 (2021) 125342.

[11] A. Mohana, S.M. Farhad, N. Haque, B. Pramanik, Understanding the fate of nano-plastics in wastewater treatment plants and their removal using membrane processes, Chemosphere 284 (2021) 131430.

[12] S. Monira, M. Bhuiyan, N. Haque, B. Pramanik, Assess the performance of chemical coagulation process for microplastics removal from stormwater, Process Saf. Environ. 155 (2021) 11-16.

[13] Z. Wang, C. Sun, F. Li, L. Chen, Fatigue resistance, re-usable and biodegradable sponge materials from plant protein with rapid water adsorption capacity for microplastics removal, Chem. Eng. J. 415 (2021) 129006.

[14] Y. Zhang, H. Jiang, K. Bian, H. Wang, C. Wang, flotation separation of hazardous polyvinyl chloride towards source control of microplastics based on selective hydrophilization of plasticizer-doping surfaces, J. Hazard. Mater. 423 (2022) 127095.

[15] Z.J. Chen, J. Fang, W. Wei, H.H. Ngo, W.S. Guo, B.J. Ni, Emerging adsorbents for micro/nanoplastics removal from contaminated water: Advances and perspectives, J. Clean. Prod. 371 (2022) 133676.

[16] M. Sajid, I. Ihsanullah, M.T. Khan, N. Baig, Nanomaterials-based adsorbents for remediation of microplastics and nanoplastics in aqueous media: A review, Sep. Purif. Technol. 305 (2023) 122453.

[17] Z.H. Wang, M. Sedighi, A. Lea-Langton, Filtration of microplastic spheres by biochar: removal efficiency and immobilisation mechanisms, Water Res. 184 (2020) 116165-116183.

[18] M.C. Shen, T. Hu, W. Huang, B. Song, G.M. Zeng, Y.X. Zhang, Removal of microplastics from wastewater with aluminosilicate filter media and their surfactant-modified products: Performance, mechanism and utilization, Chem. Eng. J. 421 (2021) 129918.

[19] Z.A. Ganie, N. Khandelwal, E. Tiwari, N. Singh, G.K. Darbha, Biochar-facilitated remediation of nanoplastic contaminated water: Effect of pyrolysis temperature induced surface modifications, J. Hazard. Mater. 417 (2021) 126096

[20] P.-L. Yen, C.-H. Hsu, M.-L. Huang, V.H.-C. Liao, Removal of nano-sized polystyrene plastic from aqueous solutions using untreated coffee grounds, Chemosphere 286 (2022) 131863.

[21] Y. Zhang, Y. Luo, X. Guo, T. Xia, T. Wang, H. Jia, L. Zhu, Charge mediated interaction of polystyrene nanoplastic (PSNP) with minerals in aqueous phase, Water Res. 178 (2020) 115861.

[22] T.F. Mastropietro, Metal-organic frameworks and plastic: an emerging synergic partnership, Sci. Technol. Adv. Mat. 24 (2023) 2189890

[23] A.A. Mohana, M. Rahman, S.K. Sarker, N. Haque, L. Gao, B.K. Pramanik, Nano/microplastics: Fragmentation, interaction with co-existing pollutants and their removal from wastewater using membrane processes, Chemosphere 309 (2022) 136682.

[24] R. Banerjee, A. Phan, B. Wang, C. Knobler, H. Furukawa, M. O'Keeffe, O.M. Yaghi, High-throughput synthesis of zeolitic imidazolate frameworks and application to CO_2 capture, Science 319 (2008) 939-943.

[25] M. Eddaoudi, J. Kim, N. Rosi, D. Vodak, J. Wachter, M. O'Keefe, O.M. Yaghi, Systematic design of pore size and functionality in isoreticular MOFs and their application in methane storage, Science 295 (2002) 469-472.

[26] G. Ferey, Hybrid porous solids: past, present, future, Chem. Soc. Rev. 37 (2008) 191-214.

[27] S. Kitagawa, M. Kondo, Functional micropore chemistry of crystalline metal complex-assembled compounds, Bull. Chem. Soc. Jpn. 71 (1998) 1739-1753.

[28] U. Mueller, M. Schubert, F. Teich, H. Puetter, K. Schierle-Arndt, J. Pastre, Metal-organic frameworks - prospective industrial applications, J. Mater. Chem. 16 (2006) 626-636.

[29] A. Phan, C.J. Doonan, F.J. Uribe-Romo, C.B. Knobler, M. O'Keeffe, O.M. Yaghi, Synthesis, structure, and carbon dioxide capture properties of zeolitic imidazolate frameworks, Acc. Chem. Res. 43 (2010) 58-67.

[30] O.M. Yaghi, M. O'Keeffe, N.W. Ockwig, H.K. Chae, M. Eddaoudi, J. Kim, Reticular synthesis and the design of new materials, Nature 423 (2003) 705-714.

[31] H. Wan, J. Wang, X. Sheng, J. Yan, W. Zhang, Y. Xu, Removal of polystyrene microplastics from aqueous solution using the metal-organic framework material of ZIF-67, Toxics 10 (2022) 70.

[32] D. You, Y. Zhao, W. Yang, Q. Pan, J. Li, Metal-Organic Framework-based wood aerogel for effective removal of micro/nano plastics, Chem. Res. Chin. Univ. 38 (2022) 186-191.

[33] M. Haris, M.W. Khan, A. Zavabeti, N. Mahmood, N. Eshtiaghi, Self-assembly of C@FeO nanopillars on 2D-MOF for simultaneous removal of microplastic and dissolved contaminants from water, Chem. Eng. J. 455 (2023) 140390.

[34] Y.J. Chen, Y. Chen, C. Miao, Y.R. Wang, G.K. Gao, R.-X. Yang, H.J. Zhu, J.H. Wang, S.L. Li, Y.Q. Lan, Metal–organic framework-based foams for efficient microplastics removal, J. Mater. Chem. A 8 (2020) 14644-14652.

[35] J. Cavka, S. Jakobsen, U. Olsbye, N. Guillou, C. Lamberti, S. Bordiga, K.P. Lillerud, A New Zirconium Inorganic Building Brick Forming Metal Organic Frameworks with Exceptional Stability, J. Am. Chem. Soc. 130 (2008) 13850-13851.

[36] J. Wang, C. Sun, Q.-X. Huang, Y. Chi, J.-H. Yan, Adsorption and thermal degradation of microplastics from aqueous solutions by Mg/Zn modified magnetic biochars, J. Hazard. Mater., 419 (2021) 126486.

[37] L.-G. Qiu, T. Xu, Z.-Q. Li, W. Wang, Y. Wu, X. Jiang, X.-Y. Tian, L.-D. Zhang, Hierarchically micro- and mesoporous Metal–Organic Frameworks with tunable porosity, Angew. Chem. Int. Ed., 47 (2008) 9487-9491.

[38] S. Abedi, A. Morsali, Ordered mesoporous Metal–Organic Frameworks incorporated with amorphous TiO2 as photocatalyst for selective aerobic oxidation in sunlight irradiation, ACS Catal. 4 (2014) 1398-1403.

[39] D. Bradshaw, S. El-Hankari, L. Lupica-Spagnolo, Supramolecular templating of hierarchically porous metal-organic frameworks, Chem. Soc. Rev. 43 (2014) 5431-5443.

[40] L. Feng, K.-Y. Wang, X.-L. Lv, T.-H. Yan, H.-C. Zhou, Hierarchically porous metal–organic frameworks: synthetic strategies and applications, Natl. Sci. Rev., 7 (2020) 1743-1758.

[41] H.Y. Guan, R.J. LeBlanc, S.Y. Xie, Y.F. Yue, Recent progress in the syntheses of mesoporous metal-organic framework materials, Coord. Chem. Rev., 369 (2018) 76-90.

[42] H. Huang, J. Li, K. Wang, T. Han, M. Tong, L. Li, Y. Xie, Q. Yang, D. Liu, C. Zhong, An in situ self-assembly template strategy for the preparation of hierarchical-pore metal-organic frameworks, Nat. Commun. 6 (2015) 8847-

[43] B. Seoane, A. Dikhtiarenko, A. Mayoral, C. Tellez, J. Coronas, F. Kapteijn, J. Gascon, Metal organic framework synthesis in the presence of surfactants: towards hierarchical MOFs?, CrystEngComm 17 (2015) 1700.

[44] L.B. Sun, J.R. Li, J. Park, H.C. Zhou, Cooperative template-directed assembly of mesoporous Metal-Organic Frameworks, J. Am. Chem. Soc. 134 (2012) 129.

[45] K.N. Kudin, R. Car, Why are water-hydrophobic interfaces charged?, J. Am. Chem. Soc. 130 (2008) 3915-3919.

[46] C. Chen, M. Zhang, Q. Guan, W. Li, Kinetic and thermodynamic studies on the adsorption of xylenol orange onto MIL-101(Cr), Chem. Eng. J. 183 (2012) 60-67.

[47] M. Hu, Y. Ju, K. Liang, T. Suma, J. Cui, F. Caruso, Void engineering in Metal–Organic Frameworks via synergistic etching and surface functionalization, Adv. Funct. Mater. 26 (2016) 5827-5834.

[48] J. Li, C. Yu, Y.-n. Wu, Y. Zhu, J. Xu, Y. Wang, H. Wang, M. Guo, F. Li, Novel sensing platform based on gold nanoparticle-aptamer and Fe-metal-organic framework for multiple antibiotic detection and signal amplification, Environ. Int. 125 (2019) 135-141.

[49] X. Ma, L. Wang, H. Wang, J. Deng, Y. Song, Q. Li, X. Li, A.M. Dietrich, Insights into metal-organic frameworks HKUST-1 adsorption performance for natural organic matter removal from aqueous solution, J. Hazard. Mater. 424 (2022) 126918.

[50] L.R. Arenas, S.R. Gentile, S. Zimmermann, S. Stoll, Nanoplastics adsorption and removal efficiency by granular activated carbon used in drinking water treatment process, Sci. Total Environ. 791 (2021) 148175-148187.
[51] S. Modak, M. Kasula, M.R. Esfahani, Nanoplastics removal from water using metal–organic framework: Investigation of adsorption mechanisms, kinetics, and effective environmental parameters, ACS Appl. Eng. Mater. 1 (2023) 744-755.

Supplementary Materials

Efficient removal of nanoplastics from water using mesoporous metal organic frameworks

Daniel Pedrero[1], Carlos Edo[2], Francisca Fernández-Piñas[2,3], Roberto Rosal[1], Sonia Aguado[1,*]

[1]Department of Chemical Engineering, Universidad de Alcalá, E-28871 Alcalá de Henares, Madrid, Spain
[2]Department of Biology, Faculty of Science, Universidad Autónoma de Madrid, E-28049, Madrid, Spain
[3]Centro de Investigación en Biodiversidad y Cambio Global, Universidad Autónoma de Madrid. Darwin 2, 28049 Madrid, Spain

* Corresponding author: sonia.aguado@uah.es

Contents:

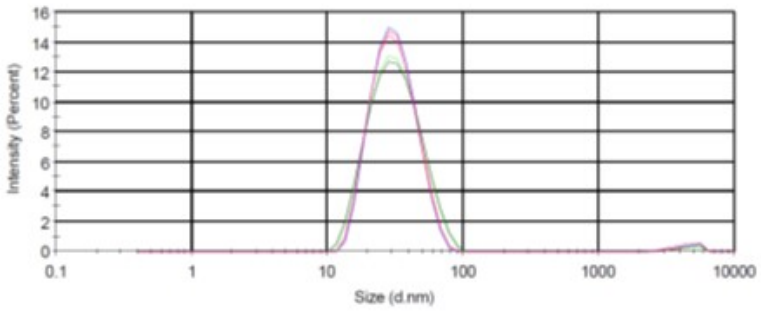

Figure S1: *DLS analysis of PS particles.*

Leaching experiments. We conducted experiments to assess the leaching behavior of the fluorescent compound. The process involved passing the solution through a 10 kDa membrane filter, followed by measuring the fluorescence of the filtered sample, the retentate sample, and the tube containing the filtered sample washed with ethanol. Additionally, we measured the fluorescence of NPs in both MQ water and at a pH of 3.

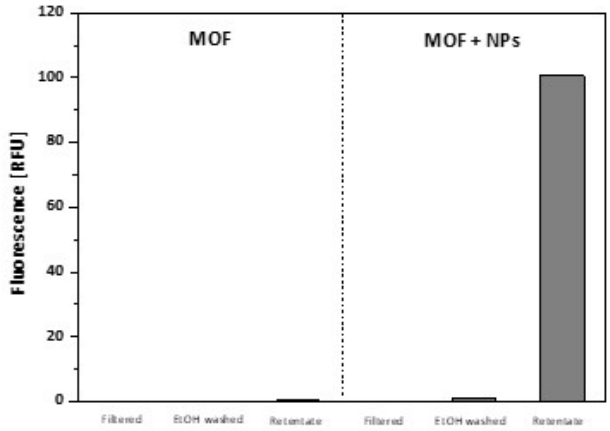

Figure S2: *Leaching experiments of UiO-66-OH/P123 (s) at 1 week.*

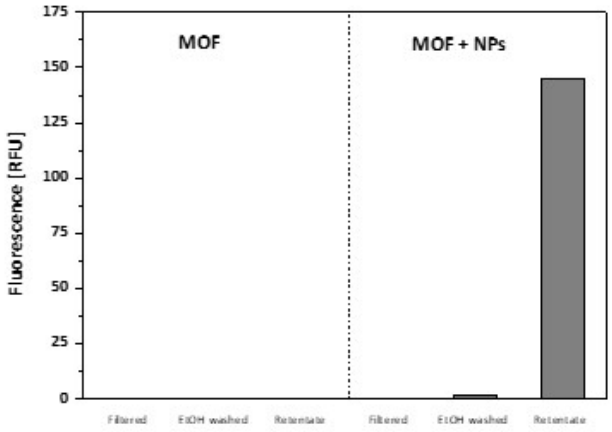

Figure S3: *Leaching experiments of UiO-66-NH2/P123 (v) at 1 week.*

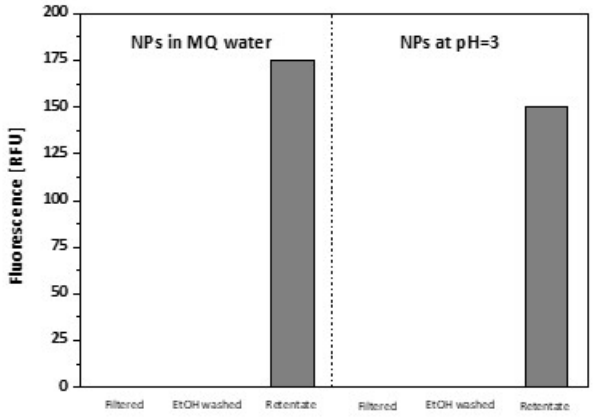

Figure S4: *Leaching experiments of NPs at 1 week.*

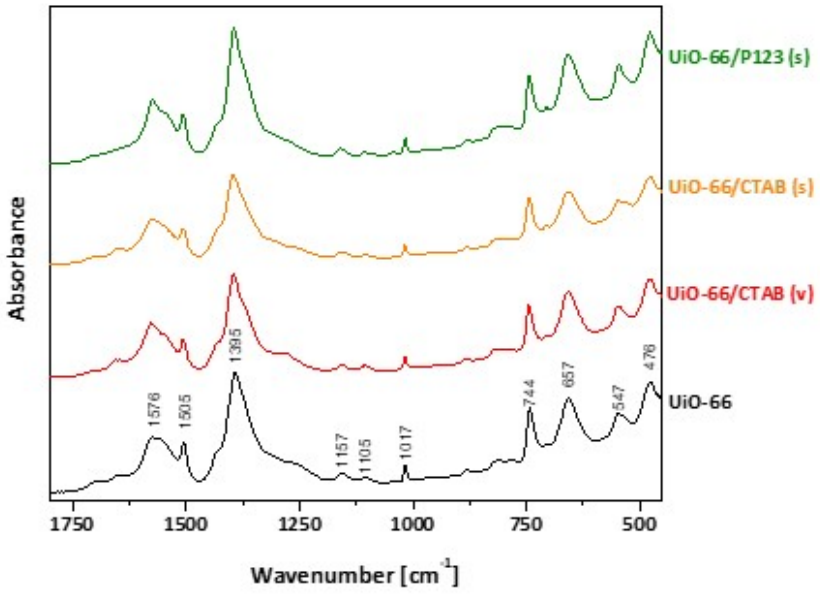

Figure S5: *FTIR of UiO-66 samples.*

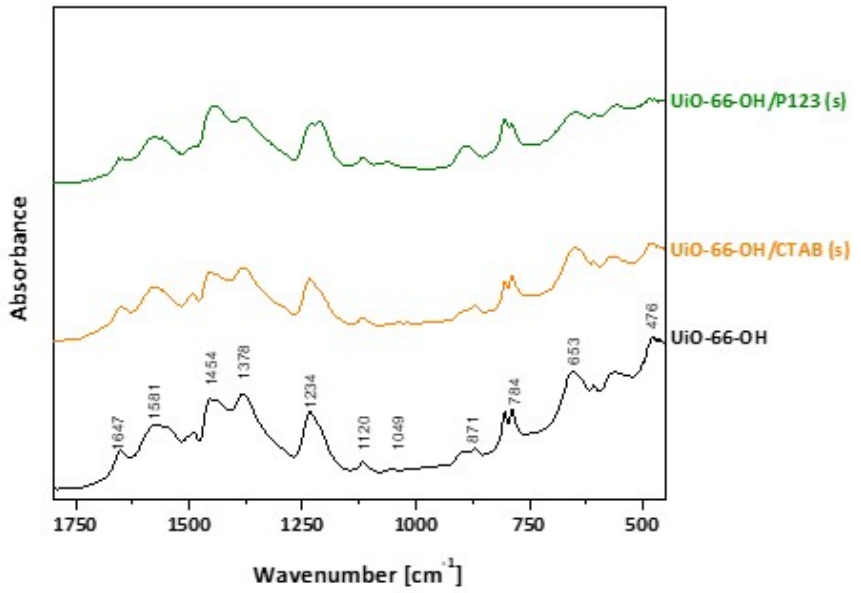

Figure S6: *FTIR of UiO-66-OH samples.*

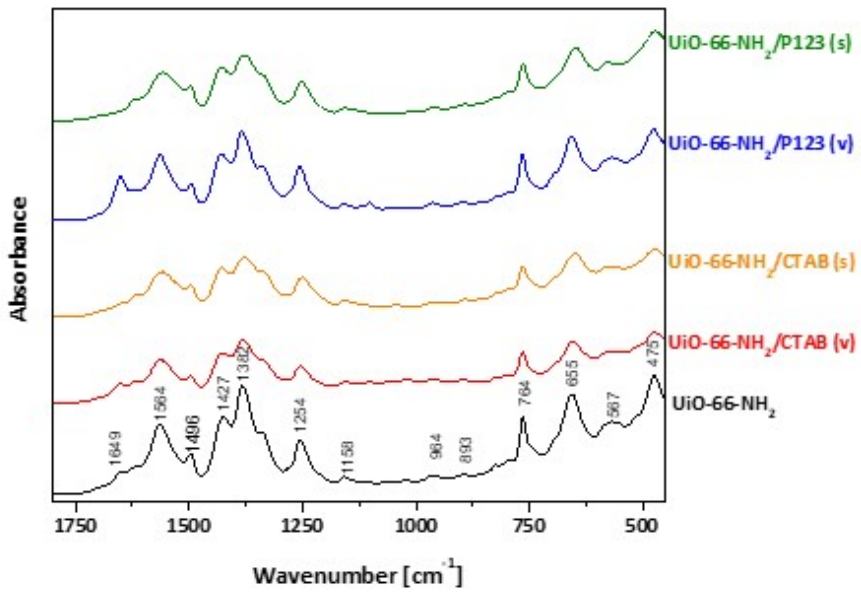

Figure S7: *FTIR of UiO-66-NH_2 samples.*